Florida Institute of Technology
Phoenix – SAE Aero Design
Final Report

Team Members:
Jeff Gibson (L)
Dan Denmark
Kathleen Murray
Steven Tucker
Ray Klingerman
Jenn Allison
Sarah Lagerquist

MAE 4292

Submitted to:
Dr. Sepri
4/25/08

I. Abstract

The SAE Aero Design competition challenges teams from many universities to design, build, and fly a model aircraft capable of lifting great loads while remaining as light as possible. Florida Institute of Technology has competed in this competition in the past. However, in recent years, teams have been unable to make it to competition in the spring semester.

The purpose of this team was to design a tandem wing aircraft that will remain light and still be able to lift a heavy payload. In order to accomplish this we must design the aircraft to be stable, structurally sound using light-weight materials, and simple to mend in the case of damage.

The team completed the construction of the aircraft and flew a successful test flight on April 15th. The team went to the competition, scored very well on the oral and written reports. During the first flight of competition, the aircraft flew most of the circuit, however it crashed when attempting to land. Analysis techniques used to design the aircraft are discussed in this report, along with possible causes of the crash.

II. Acknowledgements

The team would like to take time to thank those organizations and people who helped to make this project a success. First, without the Society of Automotive Engineers and Lockheed Martin, the competition would not have even taken place. We'd like to especially thank Lonnie Dong and Chris Dowell for running the competition and showing us their support.

We would like to thank Space Coast Hobbies for helping us troubleshoot our transmitter and supplying much of the parts and materials we required. Ace Blueprinters was instrumental in the construction of our plane, providing us with full scale drawings at no cost.

Florida Tech Facilities Management lent us a table for the entire construction process and Shipping and Receiving donated packing material for transportation purposes. The support of the campus community aided greatly throughout the course of the project.

We'd like to thank Jim Muehlen for sharing his knowledge and for conducting our first taxi test. His expertise helped us out greatly. Several other students were instrumental in our design, construction, and administrative process including but not limited to: Devin Charles, Stephan Mehling, Jake Teufert, Tim Arbeiter, and Sarah Lagerquist.

The Florida Tech Machine Shop provided us with a work area to construct the aircraft, as well as all the tools and machines necessary for the project. Special thanks goes to Bill Bailey and Ed Martin for their advice and assistance.

Finally, we would like to thank three very important individuals. Our advisor, Dr. Paavo Sepri, provided encouragement and guidance throughout the course of the entire project. His support led to our success. John Abraham, our pilot, stepped in at short notice to conduct a test flight and later flew at competition. We are forever greatful to him. Stephanie Hopper assisted in obtaining parts and materials, making numerous trips to the hobby shop, and even drove us to competition 500 miles away.

Our success lies in part with all the support we have received. Thank you.

III. Table of Contents

IV. Table of Figures

V. List of Symbols

Aerodynamics & Flight Performance

ε_1 = Downwash on the aft wing, induced by the front wing.
b = Wingspan
S = Wing Area
AR = Aspect Ratio
y (Aerodynamics) = Horizontal distance between trailing edge of mean aerodynamic chord of the first wing to the leading edge of the mean aerodynamic chord of the second wing
z = Vertical gap between both wings
λ = Taper Ratio
$\bar{c}$ = Mean Aerodynamic Chord
MAC = Mean Aerodynamic Center
α = Angle of Attack
V = Velocity
V_{stall} = Stall Velocity
V_{TO} = Takeoff Velocity
L = Lift
D = Drag
M = Moment
C_l = Section lift coefficient (infinite wing)
C_L = Finite wing lift coefficient
C_{D0} = Minimum Drag Coefficient
C_{Di} = Induced Drag Coefficient
Cm = Moment coefficient
a = $\frac{dC_L}{d\alpha}$ = Lift slope
$\frac{d\varepsilon}{d\alpha}$ = Downwash slope with respect to angle of attack
h = Longitudinal position of center of gravity with respect to the front wing MAC, normalized by the $\bar{c}$
h_n = Longitudinal position of neutral point with respect to the front wing MAC, normalized by the $\bar{c}$
i_2 = Trim angle of aft wing

Subscripts used:
1 = Property of the front wing
2 = Property of the aft wing

VI. Introduction

The aircraft designed by this team uses what is known as a tandem wing configuration. This configuration is similar to a biplane, however the wings are offset horizontally far enough that the center of gravity falls between the two lifting surfaces. Because the wings are further apart than with a biplane, it minimizes the downwash effect on the second wing. This design provides with a higher lifting capacity than with a single wing, while not increasing the overall dimensions (LxWxH) of the aircraft. The second lifting surface also provides greater stability during flight. Figure 1 below shows an overview of the design chosen:

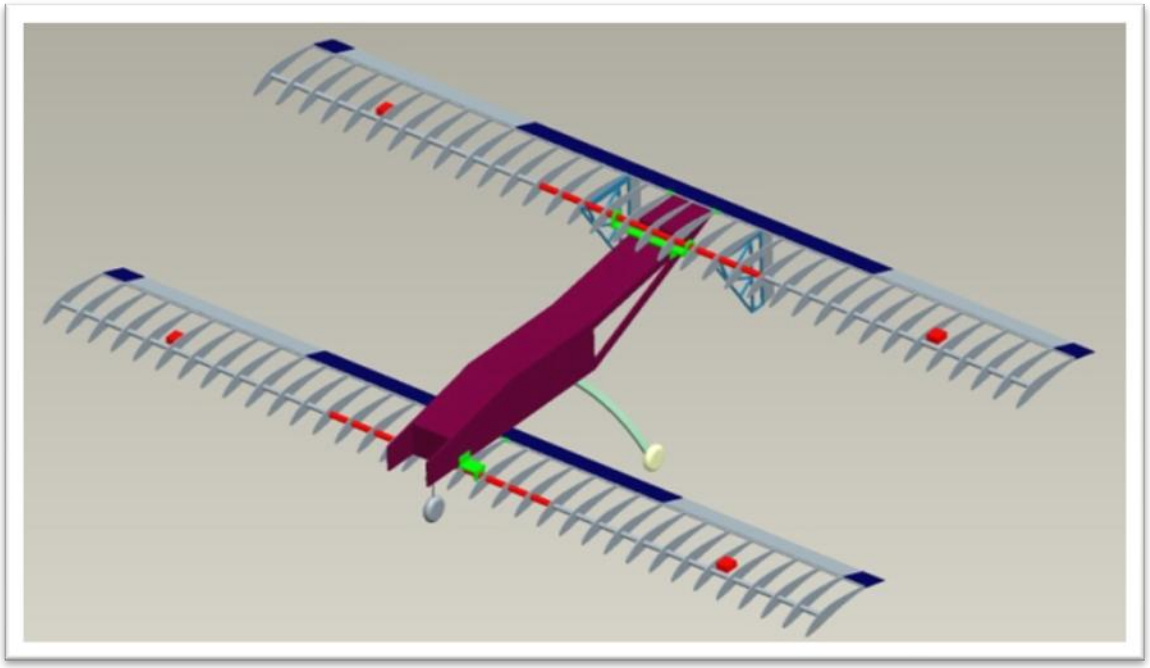

Figure 1: Design Overview

Estimated performance

- Maximum Takeoff Weight = 40.9 lb
- Total Structural Weight = 10.3 lb
- Maximum Payload (sea level) = 30.6 lb
- Stall Velocity = 37.2 ft/s
- Top Speed = 62 ft/s

VII. Payload Prediction (Steve Tucker, Jeff Gibson)

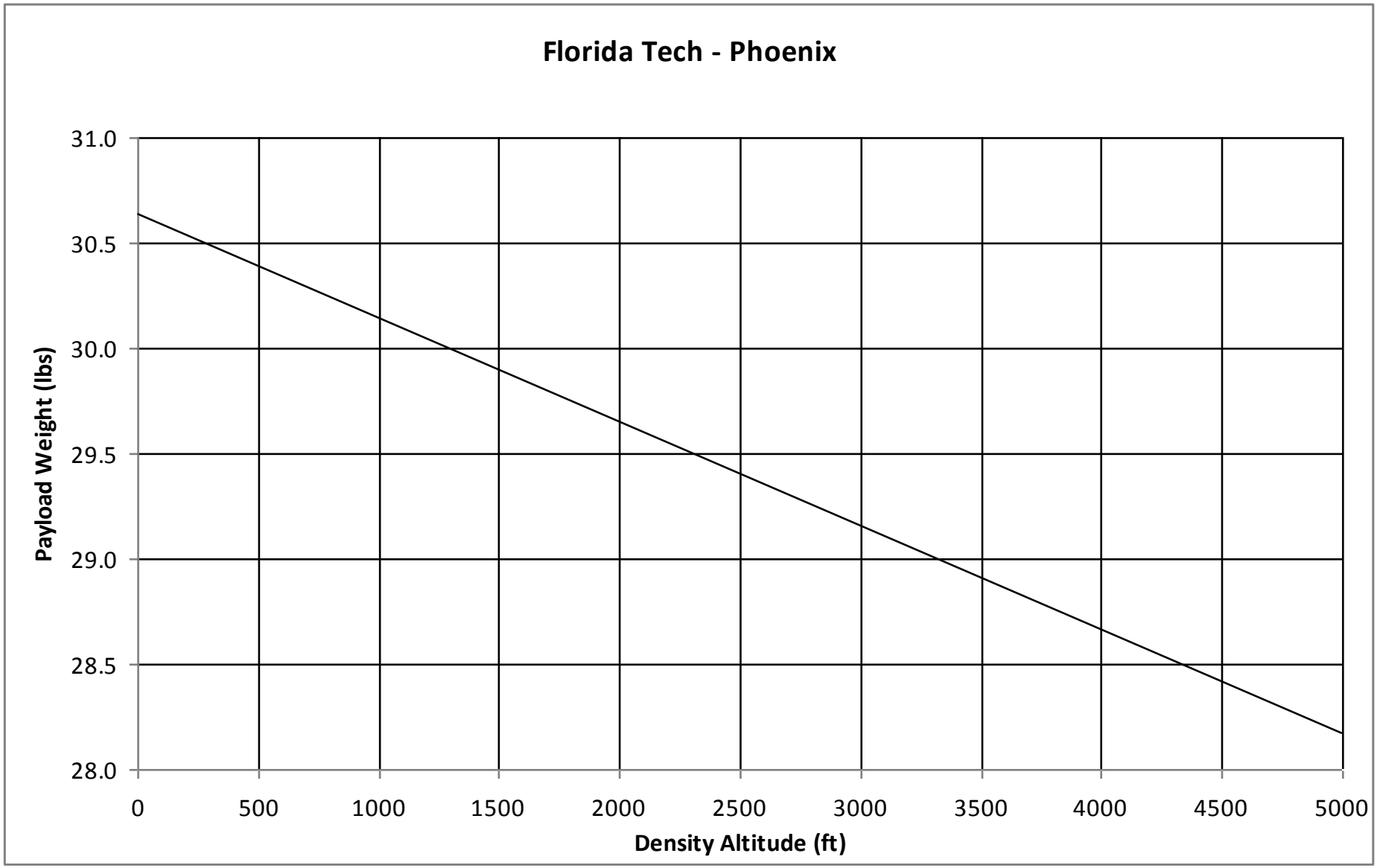

$$W_{\max} = 30.6 - (4.93 \times 10^{-4})h$$

VIII. Aerodynamic Design and Analysis

Airfoil (Steven Tucker)

The Selig 1223 airfoil was chosen for the aircraft. In comparison to other airfoils, this provides much higher lift at low Reynolds numbers (200,000~300,000). Figure 2 shows a plot of the Selig 1223:

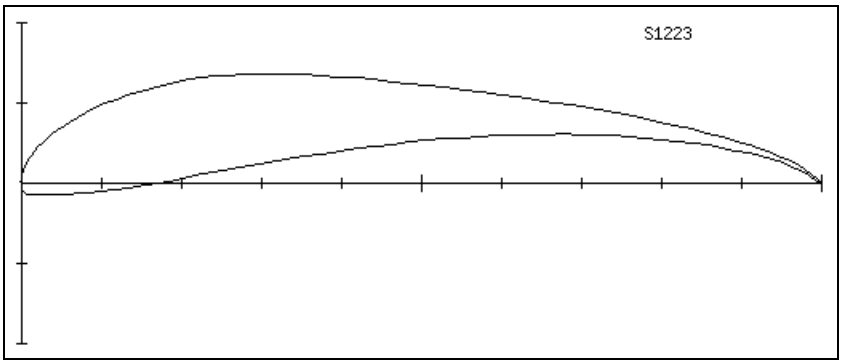

Figure 2: Selig 1223 Airfoil [1]

To obtain performance data for the airfoil, the CFD program XFLR5 was used. The lift and drag data obtained from the simulation was used in subsequent design and analysis.

Wing Planform (Steven Tucker)

When designing the wing planform, many things were taken into consideration, such as span, area, aspect ratio, planform shape, and sweep. Because the team has little model building experience, it was decided that simplified construction was also a big factor. With these aspects taken into account, a rectangular wing with no sweep was chosen. The main factors left to consider were span and chord length, and how those two factors affect the area and aspect ratio of the wing. Because the aircraft has a tandem configuration, the vertical and horizontal distance between the wings had to be taken into account as well.

When deciding on wing dimensions, it is desirable to have as high aspect ratio as possible to maximize lift. An optimization was performed to determine the optimum wing area, as well as the corresponding horizontal and vertical distance between wings, while keeping the total dimensions of the aircraft under 175 inches.

The team designed a MATLAB program that optimizes the chord length and wing area based on the take-off performance. In particular, the program analyzes the effect the forward wing has on the aft wing. The forward wing causes downwash on the aft wing, which reduces the aft wing's lift and increases its drag. The following equation 1, from E. V. Laitone's paper [2] describes the downwash angle (ω) on the aft wing.

$$\varepsilon_1 = \left(\frac{C_{L_1}}{2\pi \cdot AR_1} \right) \left[\frac{(+2y/b_1)}{(+2y/b_1)^2 + (2z/b_1)^2} + \frac{(-2y/b_1)}{(-2y/b_1)^2 + (z/b_1)^2} \right] \quad (1)$$

The longitudinal distance between the trailing edge of the forward wing and the leading edge of the aft wing is denoted as "y" in the above equation. The height difference between the tandem wings is given by "z" in the equation and "b" is the wingspan. The subscript "1" denotes the forward wing. J.H. Crowe, in his paper titled "Tandem-Wing Aeroplanes,"[4] states that the lift to drag ratio on a tandem-wing aircraft is greater than that of a single wing plane. Further, he concludes that the maximum lift to drag ratio will occur when the tandem wings are furthest apart. This is due to the fact that the downwash on the aft wing is lessened the further the wings are from each other. Due to this analysis, the team decided that the forward wing will be as close to the nose of the aircraft as possible, and the aft wing will be placed as far to the rear of the craft as possible.

To determine the optimal wingspan and chord length, the team analyzed how the take-off distance varied with an increased wingspan and increased chord length. The take-off distance can be approximated by the following equation 2, according to Leland Nicolai [3]:

$$S_G = \frac{V_{TO}^2}{a_{mean}} \quad (2)$$

$$V_{TO} = [W / (.8 \cdot S \cdot \rho \cdot C_l)]^{1/2} \quad (3)$$

$$a = (g/W)[T - D - F_C(W - L)] \quad (4)$$

The mean acceleration is taken at 70% of the take-off velocity. This affects the total lift and drag within the equation, given by the following two equations. The static thrust was taken to be 8lb, and the thrust at specific velocity was estimated using the graph in Nicolai's paper.

$$L = \frac{1}{2}\rho V_{TO}^2 S C_l \quad (5)$$

$$D = \frac{1}{2}\rho V_{TO}^2 S C_d \quad (6)$$

The coefficients of lift and drag are determined by the aerodynamic properties of the Selig 1223 airfoil as well as the aerodynamic properties of the rest of the aircraft. To approximate the drag on the fuselage, it was modeled as a rectangular box with the same frontal area, taking into account empirical data [3]. The program solves for the induced angle of attack, which is subtracted from the angle of attack of the wing. This new effective angle is then used to determine the actual coefficient of lift for a finite wing. The coefficient of lift on the aft wing is solved in the same way, except that the downwash angle must also be subtracted from the angle of attack. The lift on each wing is calculated separately and then summed for the total lift on the aircraft.

To determine the optimal chord length of the wing, the program places the leading edge of the forward wing and the trailing edge of the aft wing at a predetermined fixed position. These positions are based off the total length of the fuselage as well as other dimension requirements. The program assumes that both wings are rectangular and identical in size. Each chord length is increased linearly at the same rate. Because the leading edge of the forward wing is fixed, as the chord length grows the trailing edge moves closer to the aft wing. This occurs in the other direction for the aft wing, where the leading edge moves closer to the forward wing. As the chord length gets larger, a maximum point is reached where the aspect ratio of the wings has grown too large. At this point, the lift reduction and increase in induced drag outweigh the benefit of having a large wing area.

For each wingspan, there is an optimal chord length that maximizes the lift and minimizes the take-off distance. The following graph, Figure 3, shows how the effect on the take-off distance as the chord length grows. The data were taken at a wingspan of 8.5 ft and a gross weight of 41 pounds.

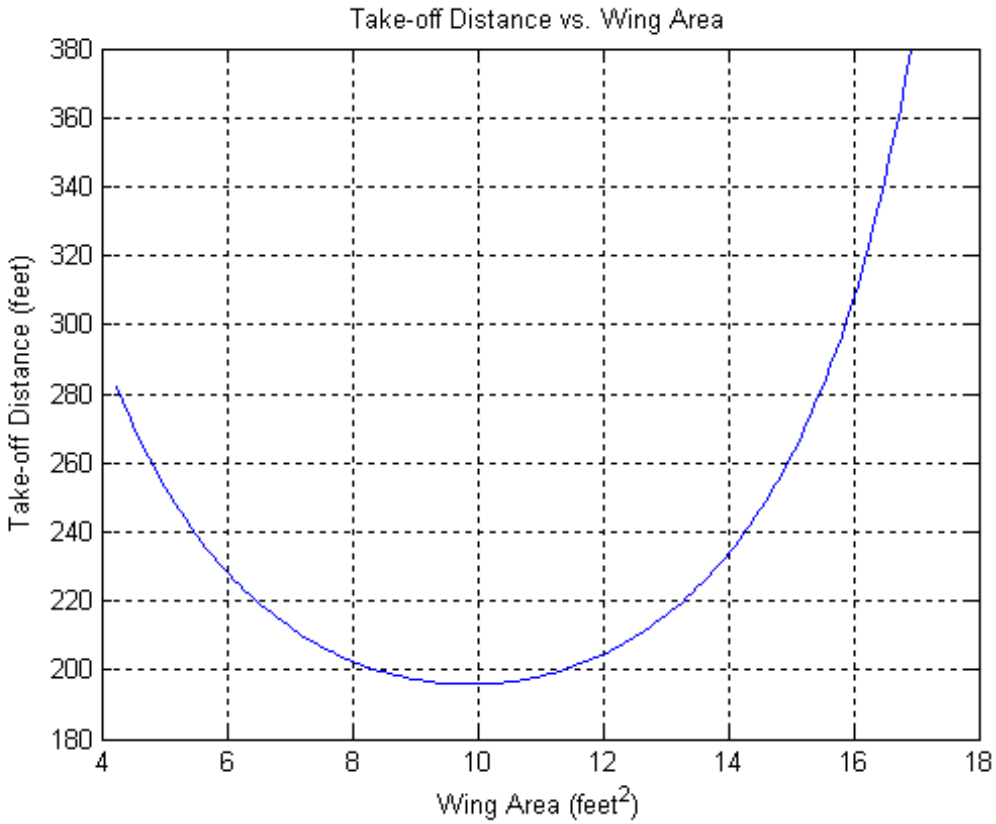

Figure 3: Takeoff distance vs. wing area for an 8.5 ft wingspan.

The optimal chord length changes as the wingspan changes as well. The program was iterated to find the optimal chord length at a range of wingspans between 8 and 10 feet and found that take-off distance decreased as the wingspan increased. Further iterations were preformed at different distances between wings. The chord length also increased as the wingspan increased. Because of structural constraints discussed later in the report, a wingspan of 8.5 feet was chosen. At a wingspan of 8.5 feet, the optimal chord length is about 1.104 feet or about 13.25 inches. At this configuration, the lift on the aft wing is 80% of that of the forward wing due to the downwash effects. The overall dimensions of this optimal configuration are 102” in wingspan, 55” in length, and 18” in total height.

Pitch Stability (Jeff Gibson)

The aircraft must be stable during flight so that the pilot can easily control it and reduce the risk of crash. This section describes the design involved to achieve static stability. Our design methodology is as follows:

1. Find the neutral point of the optimum configuration found during the takeoff analysis.
2. Place components on the aircraft to achieve a static margin of at least 5%-10%.
3. The cargo bay must be located at the center of gravity so that the C.G. does not shift as the payload is increased

The neutral point was calculated using the following formulas obtained from [5]:

$$a = a_{w_1}\left[1+\frac{a_{w_2}}{a_{w_1}}\frac{S_2}{S_1}\left(1-\frac{\partial\varepsilon}{\partial\alpha}\right)\right] \qquad (7)$$

$$h_n = h_{nwb}+\frac{a_{w_2}}{a}\bar{V}_H\left(1-\frac{\partial\varepsilon}{\partial\alpha}\right)+\frac{\partial C_{Mw}}{\partial\alpha} \qquad (8)$$

$$\bar{V}_H = \frac{S_2\bar{l}}{S_1\bar{c}} \qquad (9)$$

Where:

h_n = the distance between the mean aerodynamic chord and the neutral point, normalized by the mean aerodynamic chord.

a_{w1} = The lift slope of the front wing.

a_{w2} = The lift slope of the aft wing.

$\bar{l}$ = The distance between the mean aerodynamic centers of the two wings.

Finite wing effects were taken into account to find the reduced lift slope of both wings as follows:

$$a_{w_1} = a_{w_2} = \frac{\partial C_l / \partial\alpha}{1+\frac{2}{AR}} = \frac{5.35}{1+\frac{2}{7}} = 4.16 rad \qquad (10)$$

The slope of the downwash was found by taking the derivative of the tandem wing downwash equation with respect to angle of attack:

$$\frac{\partial \varepsilon}{\partial \alpha} = \left(\frac{a_{w_1}}{2\pi \cdot AR_1} \right) \left[\frac{\left(+ 2y / b_1 \right)}{\left(+ 2y / b_1 \right)^2 + (2z / b_1)^2} + \frac{\left(- 2y / b_1 \right)}{\left(- 2y / b_1 \right)^2 + \left(z / b_1 \right)^2} \right] \quad (11)$$

The neutral point was calculated to be 19.9" behind the leading edge of the front wing. With this in mind, movable components such as batteries, electronics, and the fuel tank were placed such that the center of gravity of the entire structure and components is located 18.2" behind the leading edge. This gives the aircraft a static margin of 12%, a very good degree of stability. At this location, the aircraft is trimmed for steady level flight at the takeoff velocity with half payload. This ensures that the aircraft will not tend to pitch forward or backwards without control input.

Vertical Stabilizer (Jeff Gibson)

The area for the vertical stabilizer was determined using the center of lateral area method [6]. Using this method, the center of lateral area of the aircraft is computed, where the area of the lifting surfaces is considered to be twice the actual value. The center of lateral area must fall at least 30% of the mean aerodynamic chord behind the center of gravity. A depiction of the lateral area is shown in Figure 4, the center of gravity (CG) and center of lateral area (CLA) are shown.

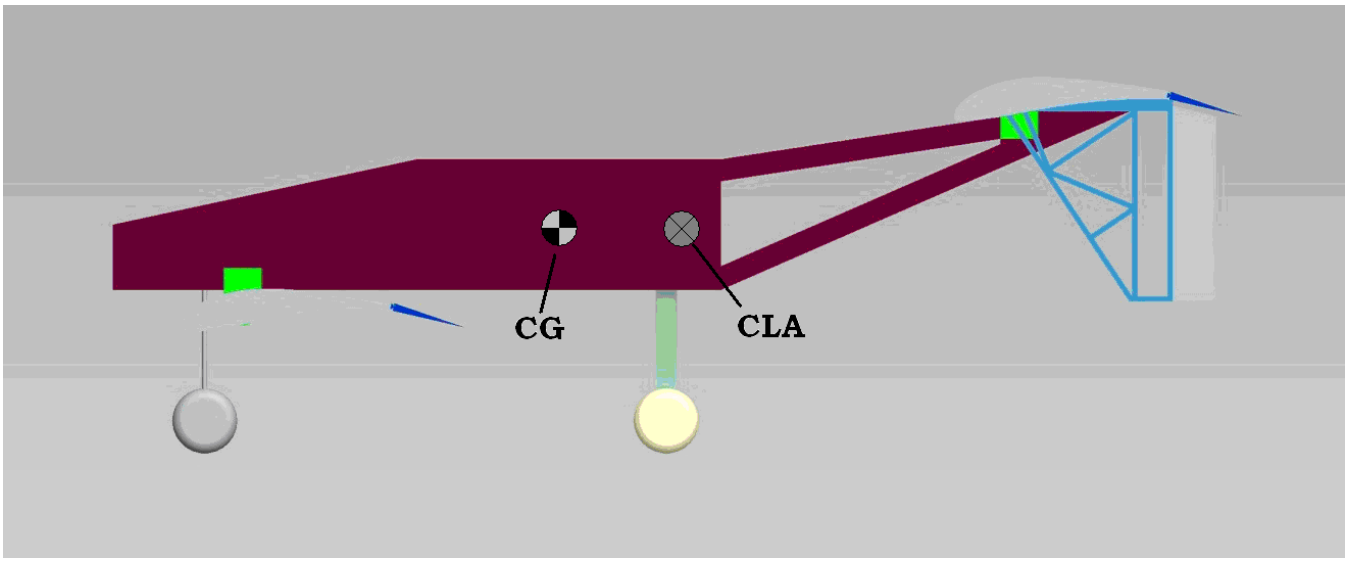

Figure 4: Center of Lateral Area

To reduce the total height of the aircraft, the horizontal stabilizer is placed below the aft wing. At this location in the center, the fin would be subject to wake from the fuselage, rendering it less effective. For this reason, it was decided to use two vertical stabilizers on each side of the fuselage, as shown in Figure 1. This configuration also allowed the stabilizers to be smaller, which provided more clearance between the stabilizers and the ground. In this configuration using the CLA method, an area of 55 in^2 was necessary for each stabilizer. The final design gave a vertical stabilizer with an area of 56 in^2.

The aircraft has a conventional control surface configuration with ailerons in front and an elevator in back. To determine an optimum size for control surfaces on the aircraft, a common "rule of thumb" was used. Most online and text resources, such as Simons[6] recommend similar guidelines for control surface sizing.

Common rules of thumb for control surface sizing:

Ailerons: 25% of the chord, 25% of the span

Rudder: 25% of stabilizer area.

Elevator: 12% of stabilizer area

Using these guidelines and rib spacing into account, the following dimensions were chosen for the control surfaces:

Ailerons: 3.46 in x 24 in

Rudders: 2 in x 8 in

Elevators: 3.46 in x 24 in (x2)

For simplicity, the elevator was split into two control surfaces identical to the ailerons, as seen in grey in Figure 5. This also allows for programming the control system to use them independently if necessary, to give more controllability.

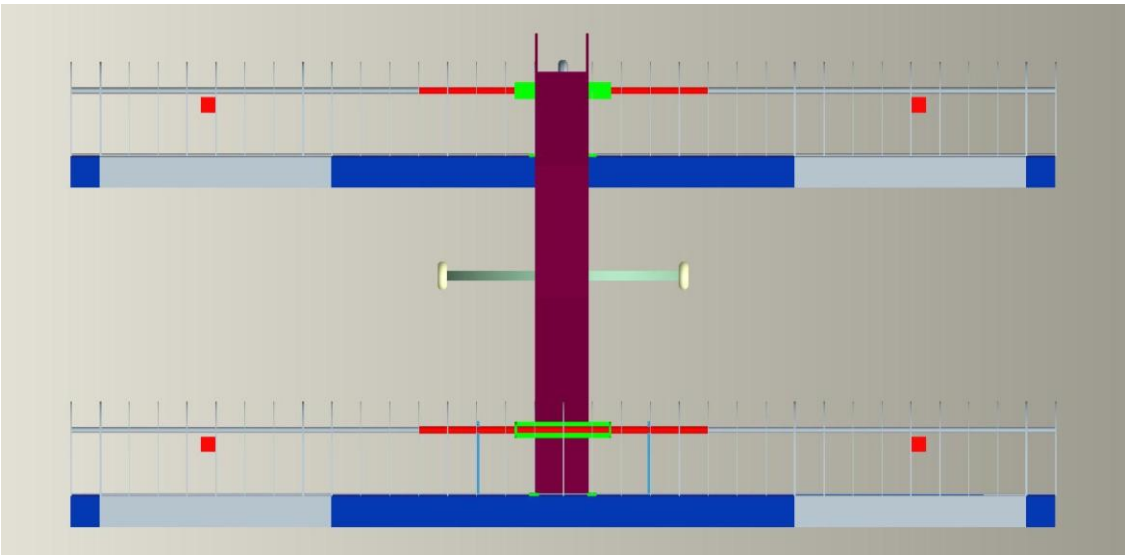

Figure 5: Control surfaces

Power Required (Steven Tucker, Jeff Gibson)

The following equation was used to find the power required for flight:

$$P_{req} = \frac{1}{2}\rho V^3 S C_{D\min} + \frac{W^2}{\frac{1}{2}\rho V S}\left(\frac{1}{\pi e AR}\right) \quad (12)$$

The power required was calculated at a range of velocities. Drag factors such as the fuselage, landing gear, tail, and wings were taken into account. Figure 6 shows the power requirement as a function of flight velocity:

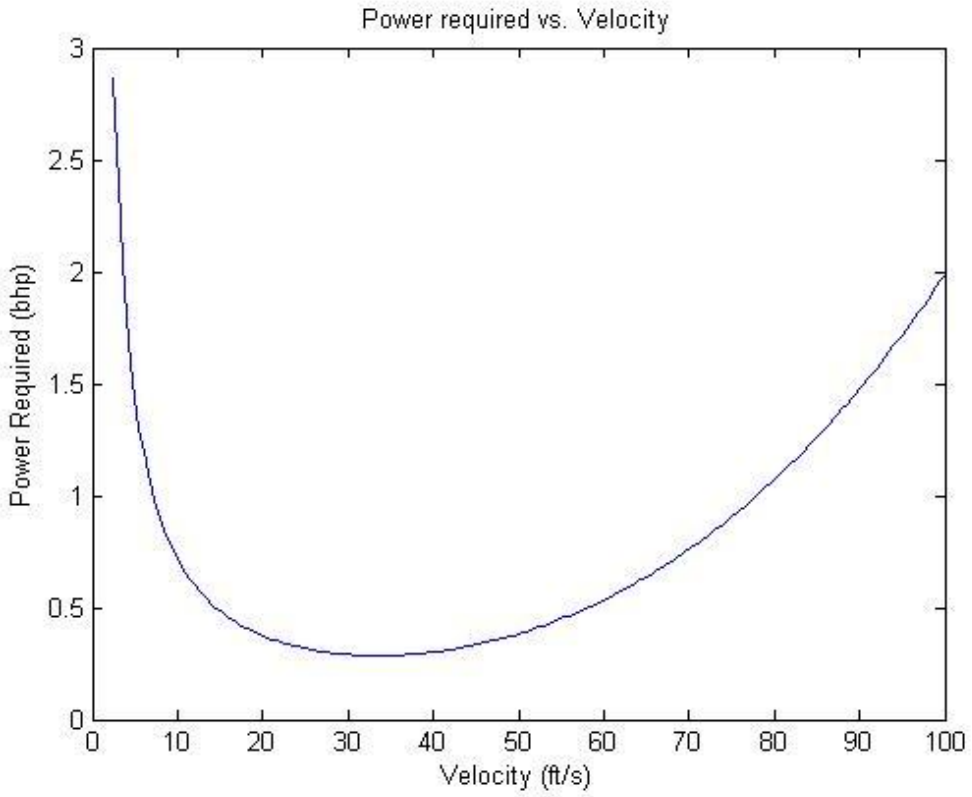

Figure 6: Power required for flight.

The minimum power required for flight is .36 brake horsepower (bhp) and occurs at the stall velocity of 37.2 feet per second at full payload. The power of the OS .61 FX engine is rated as 1.9 bhp. Thus, the engine used will be suitable for the current design.

IX. Structural Design and Analysis

The structure of the wings is an area where significant weight can be taken off by choosing the correct material, but the manufacturing methods also have to be weighed into the material decision. The first material considered was a foam which would have had carbon fiber skin and a carbon fiber spar. This material had the lower weight that the team was looking for, but it is also a very complicated manufacturing process. The second material that was considered was balsa wood for the ribs, prefabricated carbon fiber tube for the spar, and plastic sheeting called MonoKote for the skin. This method is also light weight, but the manufacturing for it will be much simpler. The team made the decision to use the second set of materials because of ease in manufacturing.

Flight envelope (Jeff Gibson)

Figure 7 shows the predicted flight envelope for the aircraft. The maximum load on the airframe is assumed to be in the theoretical case of the aircraft traveling at its maximum speed, and then abruptly pitching up to its stall angle. This maximum case of about 2 times the structural load during steady level flight corresponds to a distributed load of about 46 pounds on the front wing. The flight envelope was determined by finding the expected aerodynamic loads at velocities ranging up to the top speed of the aircraft if the control surfaces were to be fully deflected. This flight envelope was used when performing all structural design and analysis.

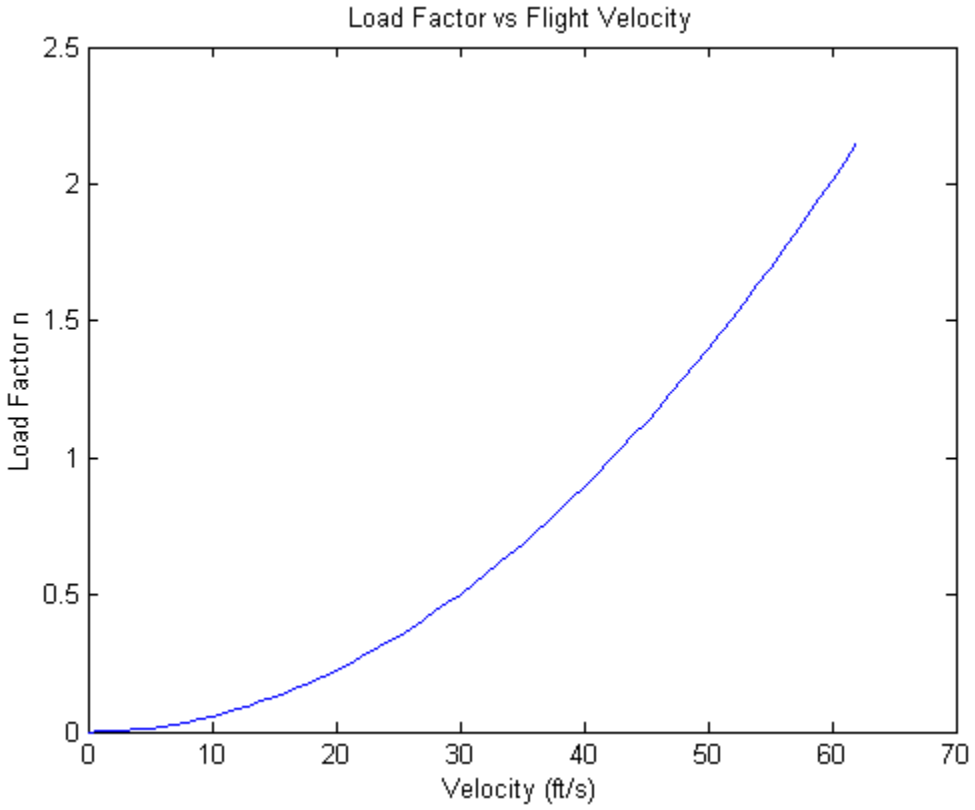

Figure 7: Predicted structural flight envelope.

Wing Structure (Kathleen Murray, Dan Denmark)

Spar

Initially the spar design began with an estimation of the loading and size in conjunction with compiling a list of desired behavior characteristics. Estimates for the size and loading came from the constraints placed by the SAE competition guidelines for the regular class competition. Those being, that the maximum weight of the loaded plane, including fuel and payload, would not exceed 55 lbs. From this a simple force balance for the plane during cruising conditions showed that the lift on the wings would be 55 lbs. This was a rough estimate used for initial calculations; more accurate design occurred later using the maximum gross takeoff weight multiplied by the load factor determined by the flight envelope.

The maximum wingspan available was estimated using the dimensional constraints given by the competition guidelines. The rules now require that each plane not exceed a 175 inch sum of the height, width and length of the plane, excluding the prop-length. From this a minimum height was estimated

based on clearance for our already existing propeller length, giving an approximate height of 18 inches. This left a maximum wingspan of 9 feet, and gave our maximum initial length for the spar design constraints.

The following list consists of the goals that were determined to have optimum performance of the spar:

- Maximize strength
- Maximize rigidity
- Minimize weight
- Manufacturing simplicity

Maximizing strength is necessary to withstand the most lift force in order to lift the most weight, which is the entire point of the competition. This strength constraint is mainly addressed by material selection but certain configurations also affected this goal and will be discussed later. Because of the long wingspan, in order to decrease any vibrations and flapping of the wings, the spar design needed to be as rigid as possible.

Besides the overall design factor of safety of 1.2 the team increased the conservative nature of the estimations by deciding that we would model the spar based on the assumption that all the lift would be absorbed by a single spar even though a secondary spar will be used to handle the torque experienced by the wing and servo/control surface placement along with increasing the overall rigidity of the structure.

Using these constraints several geometries were discussed as possible candidates for the spar geometry. Such discussion included the idea for an I-beam configuration manufactured using carbon fiber strands, which was rejected because the team felt that its fabrication experience was too low to produce something reliable within the time need to complete construction. Also, the I-beam configuration is generally used when the bending direction is fixed to maximize the I-beam properties, but the wing will be bending due to drag and lift and the resultant bending plane will shift as velocity is

varied and the I-beams behavior will be difficult to predict. Another possibility considered was a square wooden beam with carbon fiber re-enforcement, which was rejected because the square would create stress concentrations at the corners and wouldn't minimize weight. Also, the square wouldn't be a perfect square and would therefore have a preferential bending direction where it would be less resistant to bending and such a direction may not be immediately known and could result in a weak wing. Finally, a tube/cylinder design was decided upon for several reasons. First, the tube maximizes the area moment of inertia (I) of the spar while allowing for less weight, which both increases strength, rigidity and reduces weight. Secondly, a tubes bending characteristics, namely the area moment of inertia (I) is axially uniform, which is great because of the previously mentioned changing directions of the overall bending moment.

To model the bending characteristics of the wing, a simple cantilever beam model with uniform load was used.

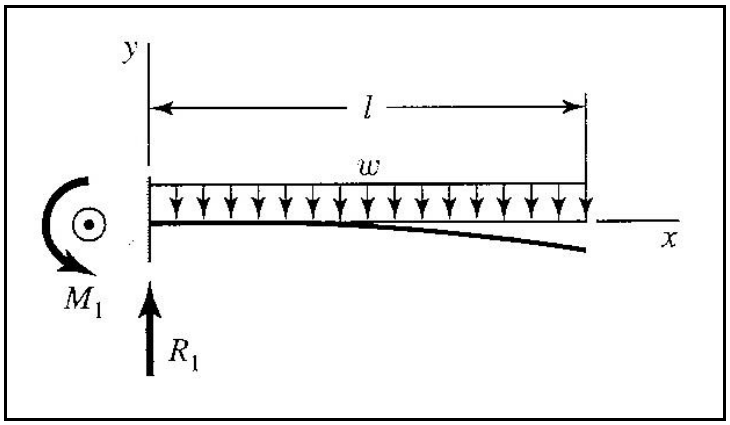

Figure 8: Cantilever beam with uniform load [8].

The uniform load was used as an approximation of the lift distribution on the wing even though the actual lift will be more parabolic and be more concentrated towards the half-spar's center. The stress and vertical displacement behavior for this configuration is

$$\sigma_{max} = 0.5\omega l^2 c/I \qquad (13)$$

$$y_{max} = -\omega l^4/8EI \qquad (14)$$

where ω is the lift distribution over the entire wing span, *l* is the length of the spar beyond the fixed end attached to the main spar bracket, E is the young's modulus for the spar's material, I is the area moment of the spars cross-section, and c is the outer radius of the spar cross-section [8].

Using this simple model the next stage was the material selection based on the goal criteria for the spar - strong, rigid, and light weight. The team compared the performance of three different materials; Carbon Fiber, Aluminum 7075-T6, and Ponderosa Pine wood. The Carbon Fiber and Aluminum can both be found in tube configurations and because we wanted to minimize weaknesses due to poor construction techniques it was decided that the Carbon Fiber would need to be purchased. Therefore it was necessary to run our calculations using cross-sections that are commercially available. Based on the 9 foot wing span and the initial cord-length it was determined that the outer diameter of the tube would have to be around 0.5-0.8 inches. A vender was found that supplied Carbon Fiber tubing with an outer diameter and inner diameter of 0.625 x 0.500 inches and with published material properties. This configuration was modeled for both Aluminum and Carbon Fiber as a comparison.

The wood couldn't be made into a tube so the cylinder configuration was selected and an outer diameter was determined based on the loading constraints, materials properties and design factor of safety. The results of the overall comparison are as follows:

	Material Properties		
	Carbon Fiber [9]	Aluminum 7075-T6 [8]	Ponderosa Pine [10]
Yield Strength [kpsi]	200	73	6.29
Allowable Stress [kpsi]	167	65.5	5.2417
Young's Modulus [Mpsi]	17.8	10.4	$1.26\text{-}1.31X10^{-3}$
Density [lbs/in^3]	0.054	0.098	0.0145
Estimated cost	$400	$60	$50
	Half-spar Analysis Results		
Stress [kpsi]	57.7	57.7	5.2417
Maximum deflection [in]	7.566	12.95	1.787
Weight [lbs]	0.3221	0.5845	0.83

Table 1: Half-spar Material Comparison Results

All of the above materials would be capable of bearing the anticipated loading conditions assumed for the comparison, but the wood weighs the most and the diameter needed to sustain the

structure was found to be 1.16 inches, which doesn't fit within our rib dimensions. The Aluminum is also heavier than the Carbon Fiber and experienced almost twice the deflection.

The final configuration of the spar is based on several factors; predicted aerodynamic loads, lengths available for purchasing carbon fiber tubes, and the addition of a coupler and bracket. The preliminary loading conditions for the final model gave a maximum stress of 55,332 psi and a maximum deflection of 7.2516 inches at the spar tip. The refined conditions gave result of 33,718 psi and 3.2066 inches while the ANSYS analysis gave results of 22,967 psi 2.4082 inches. The MatLab codes for the preliminary and final analysis can be found in Appendix A, but both are for a uniform cross-section without the necessary addition of the coupler that is included in the ANSYS analysis as can be seen below in Figure 9 and Figure 10.

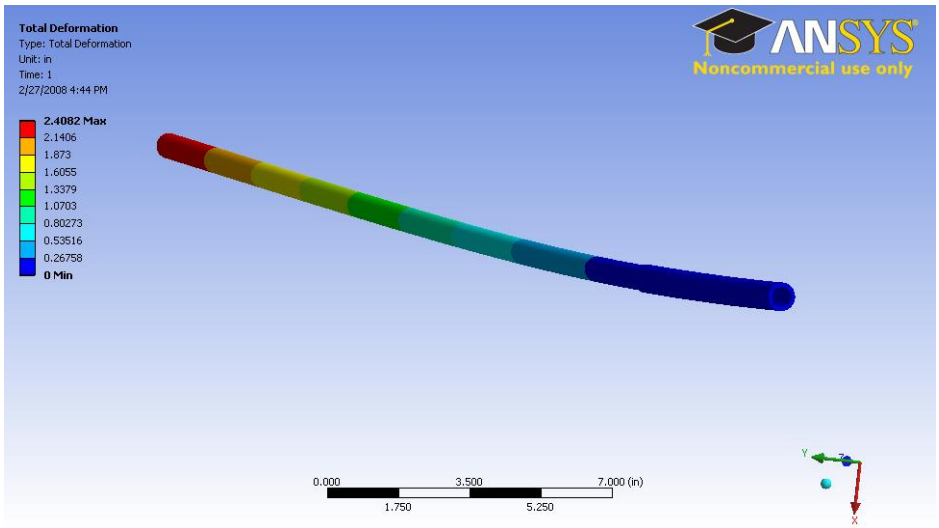

Figure 9: Spar-coupler displacement analysis using ANSYS 11.0

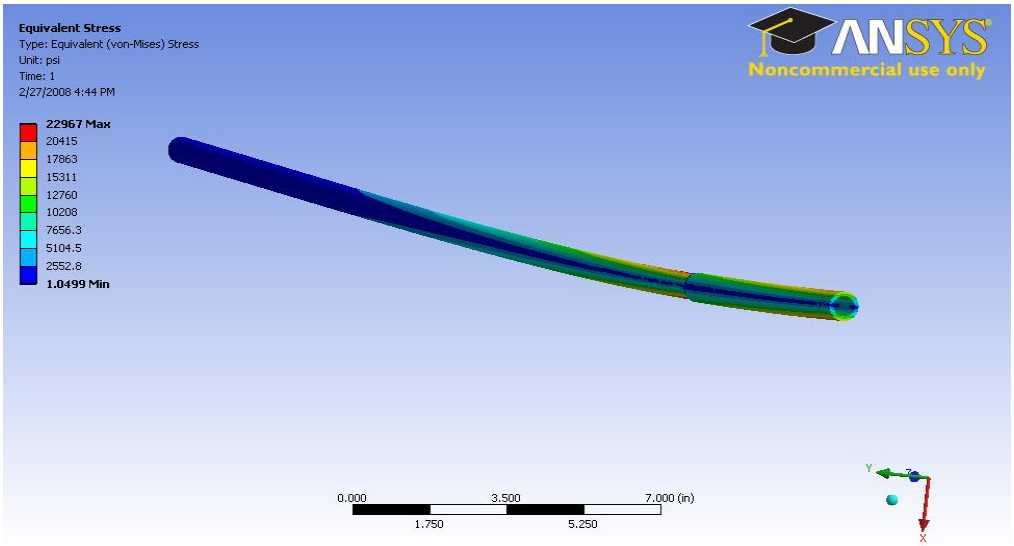

Figure 10: Spar-coupler stress

The lengths of carbon fiber tubing for the best area moment of inertia that were available commercially were 48 inches long, which would limit our wing span to 96 inches. In order to produce more lift we needed a longer wingspan, which resulted in a compromise of 8.5 feet by using a 6 inch spreader and introducing a coupler to fit the whole thing together. Tubing having an inner diameter the same as our outer diameter was found and a total coupler length of 30 inches was used in the analysis for the ANSYSIS 11.0 calculations that resulted in increasing the rigidity of our spar and decreased the maximum deflection from 3.2 to 2.4 inches. The main spar tubing was selected by finding the tubing with the largest area moment of inertia (I) available, which was a tube with outer diameter of 0.625 inches and inner diameter of 0.500 inches. The coupler, spacer and tube configuration can be seen below in Figure 11, where the spacer (having the same dimensions as the regular spar) fits in the coupler along with the ends of the main spar tubes and the whole thing can be held together using epoxy. It should be noted that the current displacement Figures are higher than the actual expected displacement because they don't account for the additional rigidity provided by the ribs, skin or secondary spar.

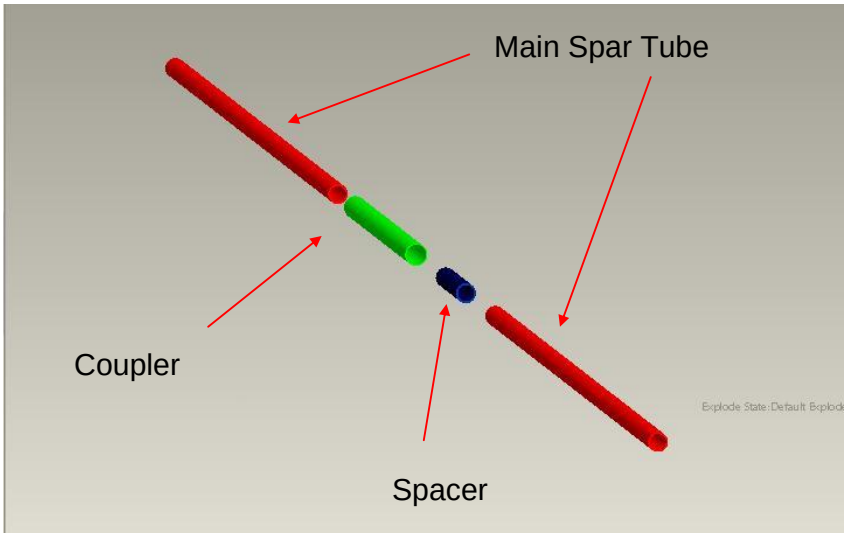

Figure 11: Spar, coupler, and spacer configuration; design by Dan Denmark.

The addition of a bracket that would absorb all the bending of the spar decreased the effective bending length of the beam (l) to 46 inches, which was taken into account in both of the final analysis calculation methods. It should be noted that the analysis results are somewhat exaggerated because the addition of the secondary spar and the ribs with the MonoKote covering will increase the rigidity of the wing and reduce the deflection.

Bracket

The design of the main spar bracket was based on the following goals:

- Capable of absorbing the bending stress from the main spar
- Able to not transmit spar stresses to the fuselage connection
- Easily manufactured

Aluminum with an allowable stress of 65 kpsi was chosen in order to meet the last goal and the resulting configuration can be seen below in Figure 12 and Figure 13, whose dimensions are 10 inches wide 0.25 inches thick and roughly 3 inches tall (including the generic fuselage connections). These dimensions were chosen because of available material configurations and the analysis results using ANSYS 11.0 indicate that the current configuration meets all our goals so there is no need to change the dimensions.

The analysis took the loading analysis from the most current lift loading provided by the aero team, the same used in the final spar analysis, and then transferring that loading using a static analysis of the wing to the surfaces of the bracket. The displacement vector sum results are shown in Figure 12.

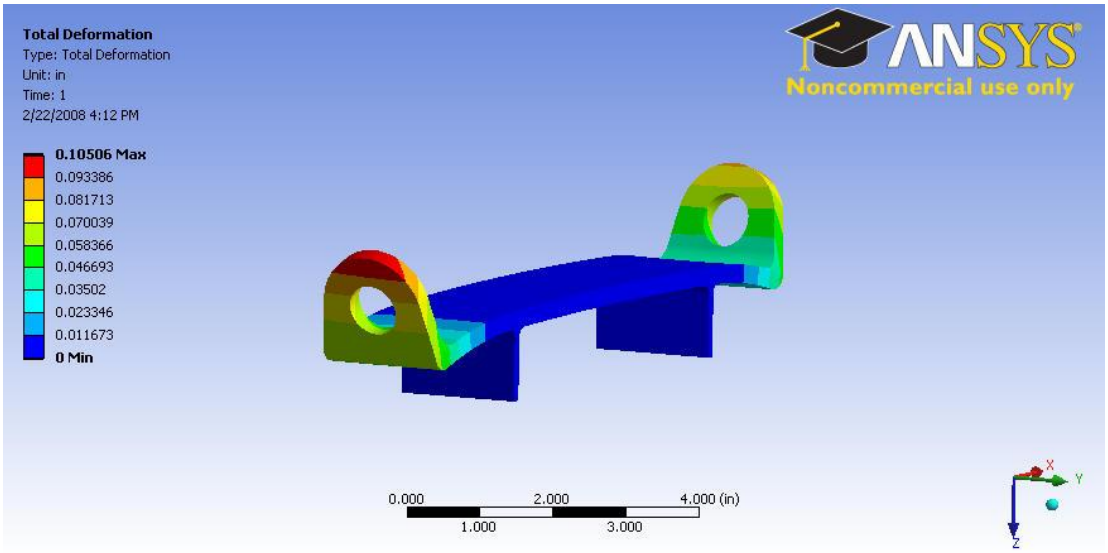

Figure 12: Main spar bracket vector sum displacement; design by Dan Denmark

The displacement is greatest at the tips as is expected and the displacement of the fuselage attachments was affectively 0, which would result in virtually no stress be transferred to the fuselage. This makes it possible to make a cheap, light weight fuselage that doesn't have to be very strong. The Von Mises stress results can be seen below in Figure 13. They indicate that a little bit of stress will be found in the fuselage attachments but the stress is small and there does need to be force transferred to the fuselage to generate the acceleration necessary for flight.

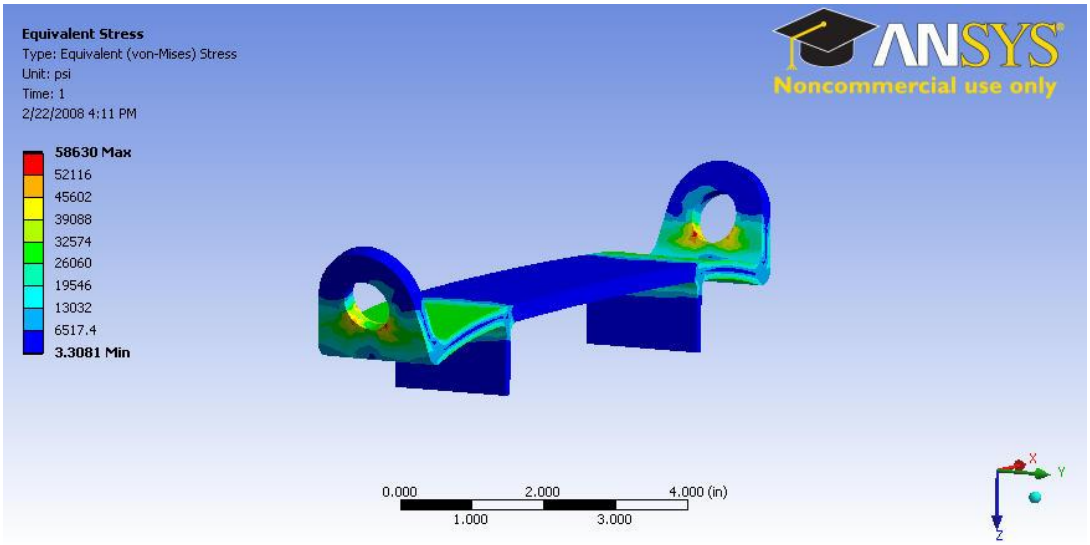

Figure 13: Main spar bracket Von Mises stress; design by Dan Denmark

Ribs and Skin

The ribs will be constructed out of pieces of balsa wood cut to the chosen airfoil shape. The shapes would be cut out by tracing the shape off of a piece of paper using a pen, and then could be cut out of the main sheet of wood using a simple razor blade. After the wing is assembled it would be covered with MonoKote by simply tacking the sheet down and then applying heat to it with an iron. The MonoKote provides several advantages over the composite layup that was discussed previously. First, the MonoKote has a simpler manufacturing process then the composite layup. Secondly, the composite material is very hard to repair if there is a problem with it, but with the MonoKote all that has to be done is reapplying the heat. If there are wrinkles it is just apply heat, for a hole there is pressure activated MonoKote to apply in the field, and then a patch can be made of the original MonoKote which is then applied with heat.

This material choice was made based on the ease of manufacturing, and it allows for varying the spacing between the ribs as the team sees fit. This spacing between the ribs can be determined by several methods including but not limited to the stress that the ribs will experience and the tension needed from the skin to hold it taught. After a literature search it was determined that initial failure due to excessive rib spacing would be buckling of the monokote skin. This failure will occur before the

spacing becomes large enough that the ribs will individually support enough force to cause failure. A spacing of 3” was chosen, as models of similar size have between 2 and 4 inch spacing.

Fuselage (Ray Klingerman)

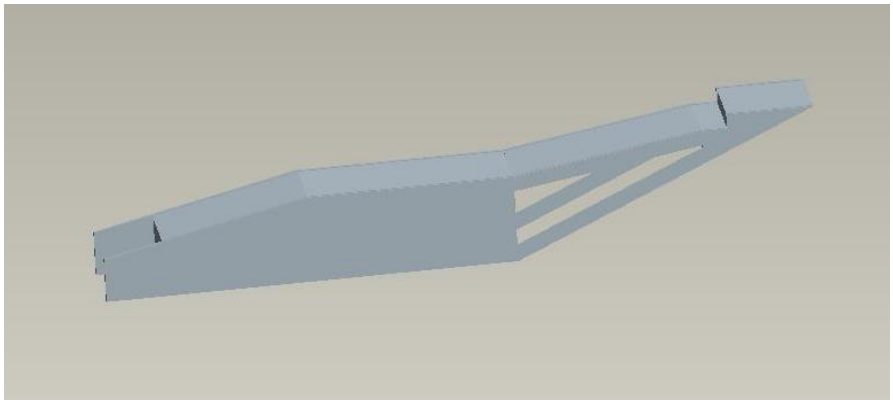

Figure 14: Fuselage drawing by Ray Klingerman

The fuselage, as shown inFigure 14, of the aircraft is made entirely of bass wood except for the fire wall which is made of plywood. The main body of the fuselage has a semi-rectangular shape with a tail section that slopes slightly upward and a nose section that has a downward slope on the top. The side of the fuselage is made of five different pieces of bass wood. The nose piece is one, the side of the main section is another, the pointed tail section is another, and there are two 1” wide tail booms. The top of the fuselage consists of three bass wood pieces that will be able to be simultaneously removed in order to access the payload, fuel tank, and other components. The bottom of the sloped tail will not be a solid piece instead it will have bass wood cross members. Each piece of bass wood is 3/16” thick. The whole fuselage will be wrapped in Monokote. The firewall is made of plywood because it is sturdier than the bass and will be able to withstand the stresses that it will undergo with the engine mounted to it. The point at the very tip of the tail will attach to the secondary spar of the rear wing supporting it and the brackets for each wing will be attached directly to the fuselage in their designated positions. The fuselage by itself will weigh no more than 3.5lbs. The inside of the fuselage has an inner width of 5” which allows the cargo box to fit tightly within. Carbon fiber rods will be added to the floor of the fuselage at the corners where it meets the walls. There will also be carbon fiber rods running from the

tail section to the main body of the fuselage. The carbon fiber rods are being used to strengthen the fuselage and support some, if not most of the stresses that the fuselage is going to experience.

Landing Gear (Ray Klingerman, Dan Denmark)

Stress Calculations

The basis behind the loading prediction for the landing gear is the impulse momentum formula which is

$$\int_0^t F(t)dt = \int_1^2 mdv \qquad (17)$$

and can be simplified to

$$F\int_0^t dt = m\int_1^2 dv \qquad (18)$$

by assuming that the initial impact force is constant. Integrating gives the landing impact force to be

$$F = m(v_2-v_1)/t \qquad (19)$$

where v_2 is zero and v_1 is the expected vertical landing velocity. One of the assumptions we're using is that the landing will be a series of square impulses as the plane hits and then bounces/hops until it rolls flat on the runway. Another assumption is that only the vertical velocity is changing as a result of the landing because friction between the wheels and runway will be slowing down the horizontal component of the planes velocity. Also, the initial impact should be the shortest and absorb the most energy, leaving subsequent impacts to have a lesser magnitude of landing force. Based off these assumptions two charts were made to determine the landing force based on the how long the initial impact lasted. As seen in Figure 15 and 16, below, the estimated range is from 0 to 1 second, but the model becomes invalid after it reaches the static deflection caused by the weight of the plane. It should be noted that while the graphs are for different velocity angles the actual angle of the airplane will have to be approximately horizontal and slightly tilted back for a landing to actually work. The angle referred to here is the angle of the velocity vector for the plane, which is assumed to be no more than 30 degrees at max. The landing velocity was estimated as 1.3 times the stall speed giving a value of 45.5 ft/s.

Using these two charts the landing force used in the ANSYS 11.0 analysis was 290 lbs, the maximum landing force possible. Loading and configurations for that analysis can be found in appendix A, while the Matlab code for the landing force graphs can be found in appendix D.

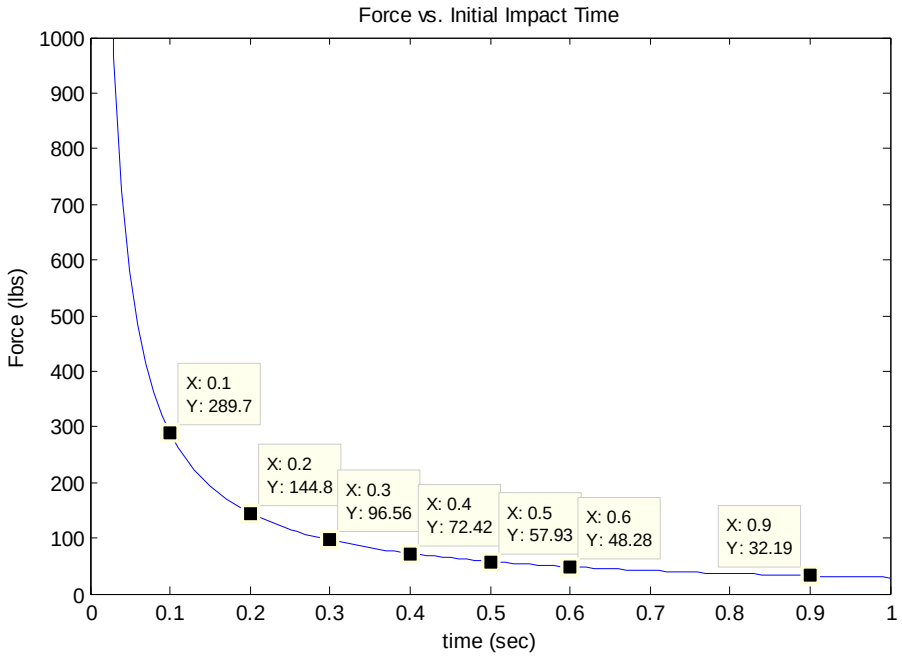

Figure 15: Landing force vs. impact time for a downward velocity angle of 30.

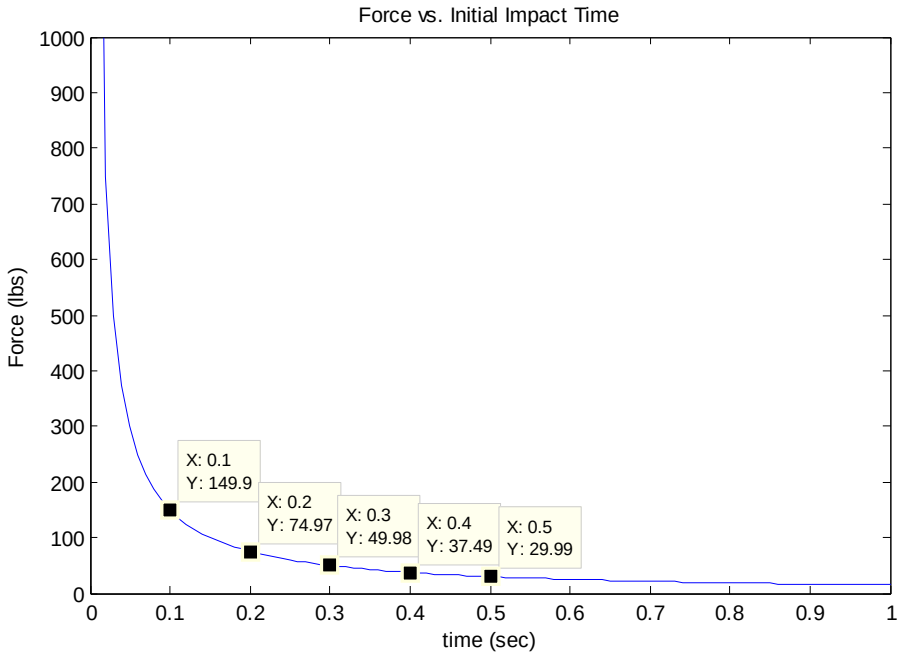

Figure 16: Landing force vs. impact time for a downward velocity angle of 15.

Landing gear design

The landing gear that is being used, shown in Figure 17, was purchased from an online carbon fiber rc-plane landing gear company named Graph Tech. The landing gear is 5.875” tall, 0.1875” thick, a wheel base of 17.75”, and a width of 17.75”. The landing gear is made of carbon fiber and was pre-manufactured for an rc kit airplane that is already in existence and was chosen due to its measurements being very close to the size that was needed for the aircraft. The size of the gear allows it to be mounted anywhere under the fuselage and the wide wheel base allows for better stability of the aircraft while on the ground. This concept weighs approximately 0.2lbs and is thin enough to not cause a sufficient amount of drag. The landing gear will be able to withstand the stresses that it will undergo during a semi-hard impact landing as the ANSYS analysis seen in Figure 18 shows. The analysis showed that the gear will experience a maximum von Mises stress of 64373 psi, which is well below the failure stress of the carbon fiber that is being used. The displacement of this was also very low, at a measurement of 0.74292”. This displacement is allowable due to the fact that there is 2 inches of clearance that allows for such bending of the landing gear. This gear appears to be easily attachable and removable if needed during the competition. The landing gear is light and durable and a perfect design for the aircraft.

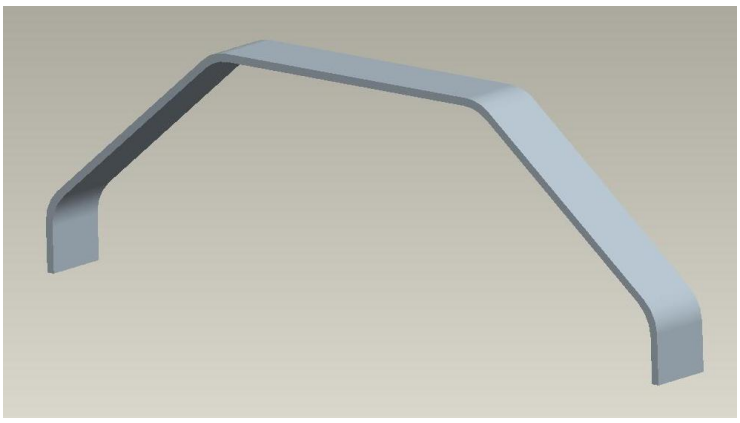

Figure 17: Landing gear

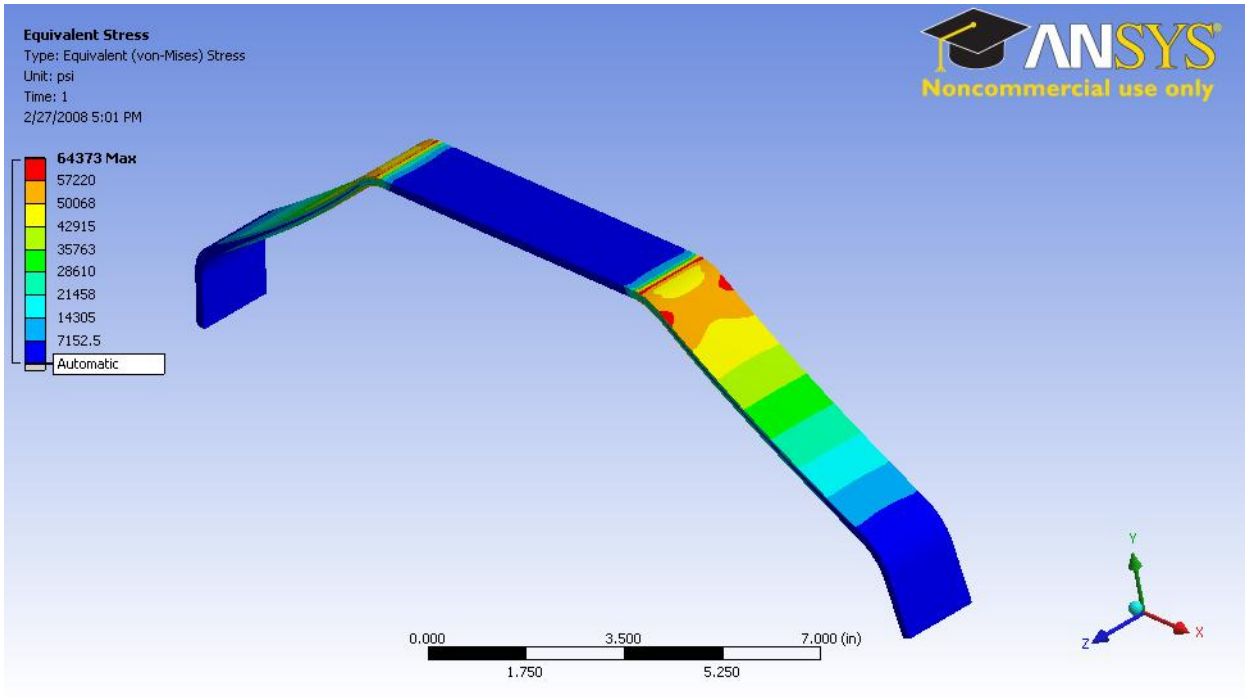

Figure 18: Landing gear analysis for Von Mises stress

Payload Assembly (Jenn Allison)

The payload assembly consists of a basswood box with two vertical bolts, shown in Figure 19 below:

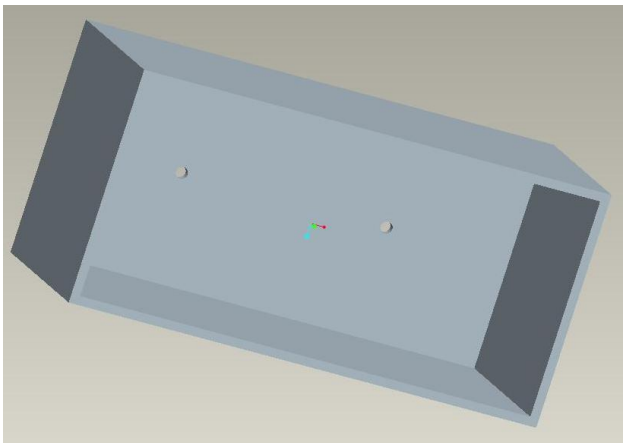

Figure 19: Payload Assembly

Payload Plates

For the payload plates used in competition, the team decided upon a simple rectangular design that will fit snugly into the cargo box. They will also have two holes drilled in them to allow for the support pegs to hold them in place. Several different sizes of plates will be made to allow the team to increase the payload easily during competition.

The team will be using scrap steel from the machine shop to make its payload plates. Using this material, the plates will have the following dimensions:

Weight	Quantity	Thickness (in)	Length (in)	Width(in)
1	4	0.25	3.2	4.25
5	3	0.5	8.2	4.25
10	3	1	8.2	4.25

Table 2: Payload Plate Dimensions

X. Control Systems

The aircraft uses a Futaba T7CHP transmitter and a Futaba R149DP receiver. In order to ensure that the servos used to control the aircraft are of adequate size, the following calculation was performed:

$$T = 8.5E\text{-}6 * (C^2 V^2 L \sin(S1) \tan(S1) / \tan(S2)] \quad (20)$$

Where:

T = servo torque in inches

C = Control surface chord in cm

L = Control surface length in cm

V = Speed in MPH

S1 = Max control surface deflection in degrees

S2 = Max servo deflection in degrees

For the calculation, the airspeed was assumed to be the top speed of the aircraft (40mph). A conservative assumption would be that the servo and control surface deflection is no more than 45 degrees. Using these parameters, it was determined that the maximum torque required for both the ailerons and the elevators would be 50.6 oz-in. The servos purchased are rated at 168 oz-in at 6 volts. For each rudder, 6.4 oz-in of torque is required, which will be fulfilled by a single servo rated at 49 oz-in.

XI. Budget Overview

Item	Total
Basswood	$53
Balsa	$75
Carbon fiber	$464
Monokote Sheeting	$94
Epoxy/Model Glue	$31
Miscellaneous Parts	$100
Tools	$100
Electronics	$686
Registration Fee	$450
Travel Expenses (hotel,gas)	$700
Total	**$2,753**

Table 3: Budget Overview

As seen in Table 3, the final cost of the project was $2,753. This was slightly under the original predicted budget. Most of the cost incurred was in the electronics, the carbon fiber, and the registration & travel fees.

XII. Plan and Schedule

As seen in Figure 20, the aircraft was completed as planned. There were delays within the last few weeks before competition due to failure of the radio system. After these issues were resolved, the test flight was successful, carrying a payload weight of 7 pounds.

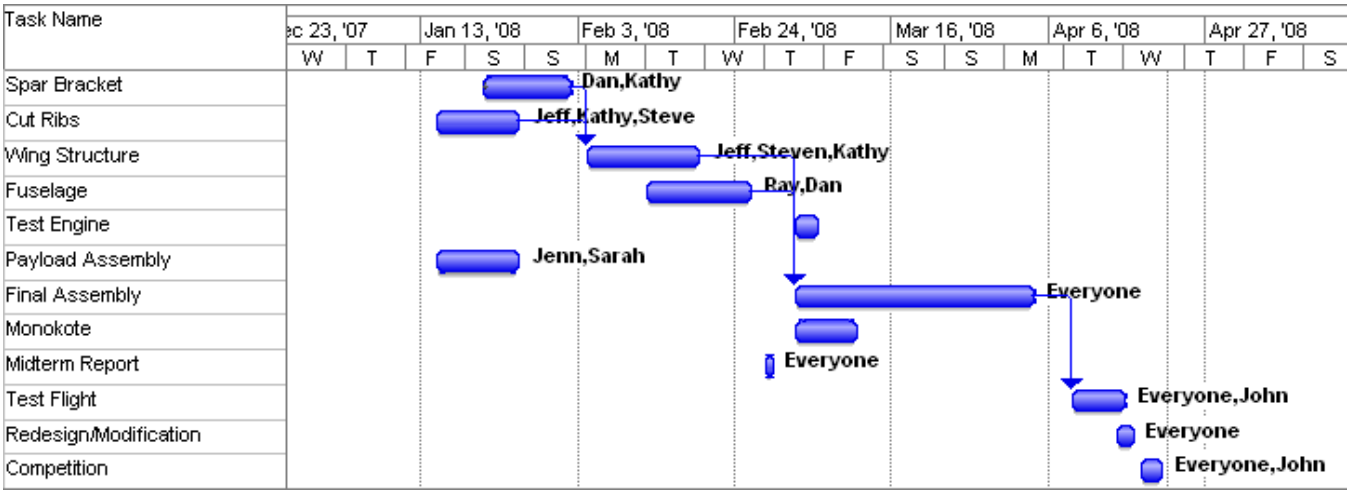

Figure 20: Schedule

XIII. Competition Results

- Placed 22nd out of 39, regular class
- 2nd out of teams without a flight score
- 16th place Oral/Written reports

During the first flight of the competition, the team attempted a bonus empty flight. After making a circuit of the airfield, the plane was coming in for a landing, then suddenly went into a steep dive, crashing into the ground. During the dive, the pilot was inputting full up elevator, but the aircraft did not respond. Possible reasons for failure are listed below:

1. **Torsion in fuselage due to wings**

Though most likely not the cause of failure, the fuselage tended to torque during flight, usually when the aircraft banked into turns. This did`n't seem to have any direct influence on the flight characteristics of the aircraft, but should be avoided in the future.

2. **Modified CA hinges**

During the technical inspection, the judges deemed that the control surfaces on the aircraft were not properly bonded to the carbon fiber secondary spar. To fix this, the team used fishing line to sew the hinges more securely to the spar, eliminating the possibility of flutter of the control surfaces. The surfaces were checked to ensure that they had full range of motion, however they may still have been restricted enough to reduce the pitch authority of the aircraft.

3. **Radio interference**

The aircraft used a 2.4Ghz radio system, so while interference from other radio systems is unlikely, there may have been interference from other sources that could have caused the loss of control. Systems like cordless phones and wireless computer networks also share the same 2.4Ghz radio band.

4. **Overloaded battery**

If enough of the servos were working at the same time, it is possible that the battery power was not adequate enough to allow the full deflection of control surfaces. The sudden pitch down seen during the test flight may have been either the servos or the receiver momentarily losing power.

5. **Speed Instability**

It is possible that the tendancy for the aircraft to pitch forward was affected by velocity. If this was the case, as the aircraft would pick up speed, the pilot would have to give a greater degree of up elevator to keep the plane trimmed. If the aircraft were to reach a certain critical velocity, the pitch authority provided by the elevators would no longer be enough to keep the plane trimmed. At this point, the plane would pitch forward, causing it to gain additional velocity, and pitch forward even more.

XIV. Recommendations

After the completion of the project, the team reccommends the following for future teams:

1. **Laser cut ribs**

Because of the inconsistancy of cutting ribs by hand, it is recommended that future teams look into getting the ribs laser cut. This allows for a more precise airfoil shape and makes applying the monokote much easier. Laser cut ribs are also much less time consuming.

2. **Additional research into control schemes**

The crash at competition may have been avoided if the ailerons also served complementary to the elevators. This would have given the aircraft a greater ability to control it's pitch. Further research into possible control schemes would prove beneficial.

3. **Verify battery power is adequate**

In order to verify that the battery used is adequate to power the receiver and all servos onboard the aircraft, additional testing of the control system electronics is necessary.

4. **Increase torsional rigidity on fuselage**

If a smilar design is persued in the future, the fuselage structure must have adequate torsional rigidity to support differential loads between the wings.

5. **Balsa leading and trailing edges**

To facilitate easier and more consistant application of the wing skin, it is reccomended to use thin sheets of balsa bent around the leading edge. CA hinges also work much better when bonded to balsa or basswood, so using these materials for the trailing edge of the main wing structure would be beneficial.

XV. References

[1] Selig, Michael. UIUC Airfoil Data Site. "Coordinates Database." <http://www.ae.uiuc.edu/m-selig/ads/coord_database.html>. July, 2006.

[2] Laitone, E.V. Prandtl's biplane theory applied to canard and tandem aircraft AIAA Vol 17, No4, April 1980 pg 233-237

[3] Nicolai, Leland M. "Estimating R/C Model Aerodynamics and Performance." June 2002.

[4] Crowe, J. H. "Tandem-Wing Aeroplanes: An Examination of the Characteristics of this Type of Wing Arrangement." Aircraft Engineering. October, 1935.

[5] Etkin, Bernard and Lloyd Duff Reid. Dynamics of Flight: Stability and Control. 3rd ed. Wiley: 1995

[6] Simons, Martin. Model Aircraft Aerodynamics. Biddles Ltd, Guildford and King's Lynn. 1999.

[7] Budynas, Richard: Mechanical Engineering Design, 8th ed., McGraw-Hill Book Company, NY, 2007.

[8] Beer, Ferdinand: Mechanics of Materials, 4 ed., McGraw-Hill Book Company, NY, 2006.

[9] GraphiteStore.com. <http://www.graphitestore.com>. Copyright 2002-107. September, 23rd 2007.

[10] Automations, Inc. http://www.matweb.com/search/SpecificMaterial.asp?bassnum=PTSAJ Copyright 1996-2007. September 25th 2007.

[11] Fieldman, Jim. "Servo Torque Calculations" Electric Flight in Colorado. <http://www.csd.net/~cgadd/eflight/calcs_servo.htm>. December 18, 2007.

Appendix A: Analysis of Structures

I. Preliminary Spar Analysis

```
dens =0.054;                %lbs/in^3
Do = 0.625;                 %in
Di = 0.5;                   %in
L = 54;                     %in
E = 17.8E6;                 %psi
w = 58/108;                 %lbs/in load uniformly distributed over entire wing length
A=(pi/4)*(Do^2-Di^2)        %in^2
weight=dens*A*L*2           %lbs
I = (pi/64)*(Do^4-Di^4)     %in^4
stress = (w*Do*L^2)/(4*I)   %psi
y = (w*L^4)/(8*E*I)         %in
```

Results

```
weight = 0.6441
I = 0.0044
stress = 5.5332e+004
y = 7.2516
```

II. Final Spar Analysis

```
dens =0.054; %lbs/in^3
Do = 0.625;  %in
Di = 0.5; %in
L = 46; %in
E = 17.8E6;  %psi
w = 46/102;  %lbs/in load uniformly distributed over entire wing length
A=(pi/4)*(Do^2-Di^2)  %in^2
weight=dens*A*L*2  %lbs
I = (pi/64)*(Do^4-Di^4)  %in^4
stress = (w*Do*L^2)/(4*I)  %psi
y = (w*L^4)/(8*E*I) %in
```

Results

```
weight = 0.5368
I = 0.0044
stress = 3.3718e+004
y = 3.2066
```

III. Ansys 11.0 loading and constraints

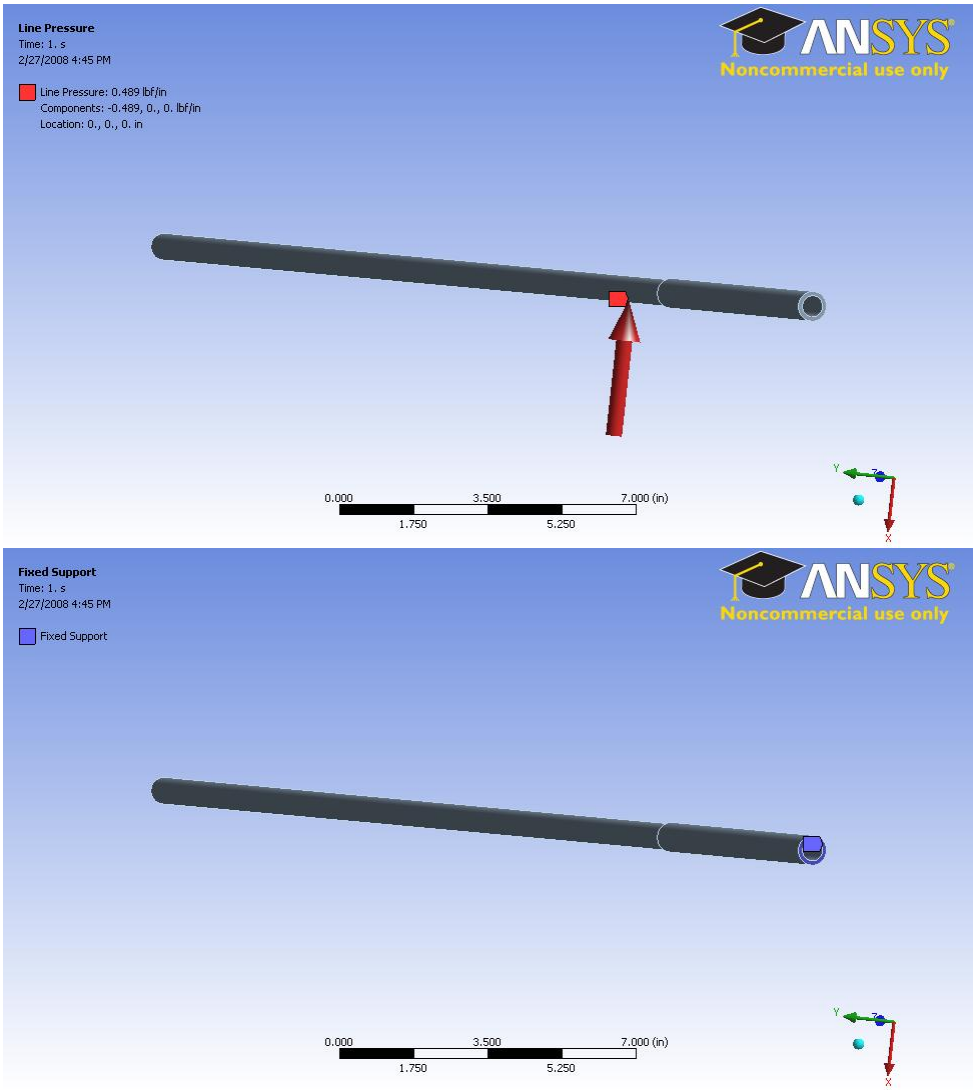

Figure 21: Constraints placed on analysis of beam.

The above image illustrates the constraints placed on the Ansys 11.0 analysis of the beam. The red arrows represent the lift distributed over each node of the wing, 22.5 lbs/in and the blue square indicates the rigid connection with the bracket.

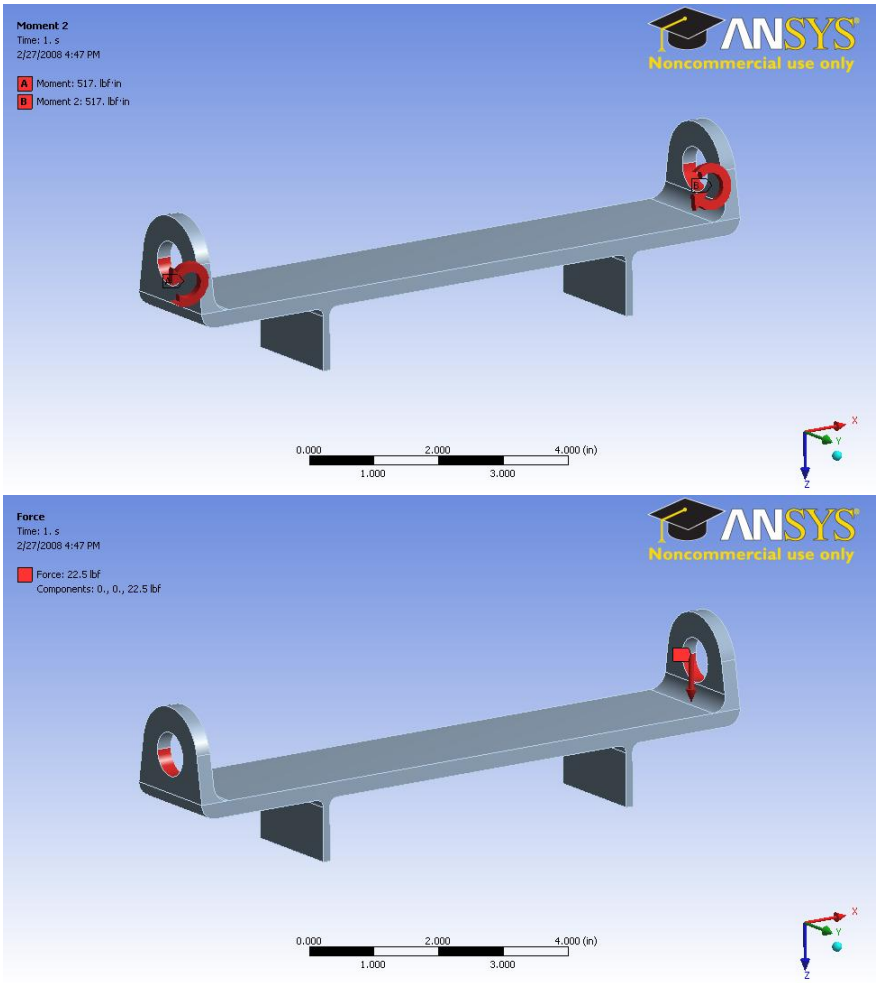

Figure 22: Loading conditions on spar bracket, ANSYS 11.0 by Dan Denmark.

The above image is the loading the conditions placed on the main spar bracket. The red arrows are the reaction forces placed on the hole by beam, and the red circular arrows indicate reaction moments at the ends. The forces used were determined by a static analysis of the wing where the lift force on a half-spar of 22.5 lbs was transferred to the outer edge of the main spar bracket hole. The moments were determined from the ANSYS 11.0 analysis of the beam and were 517 lb*in.

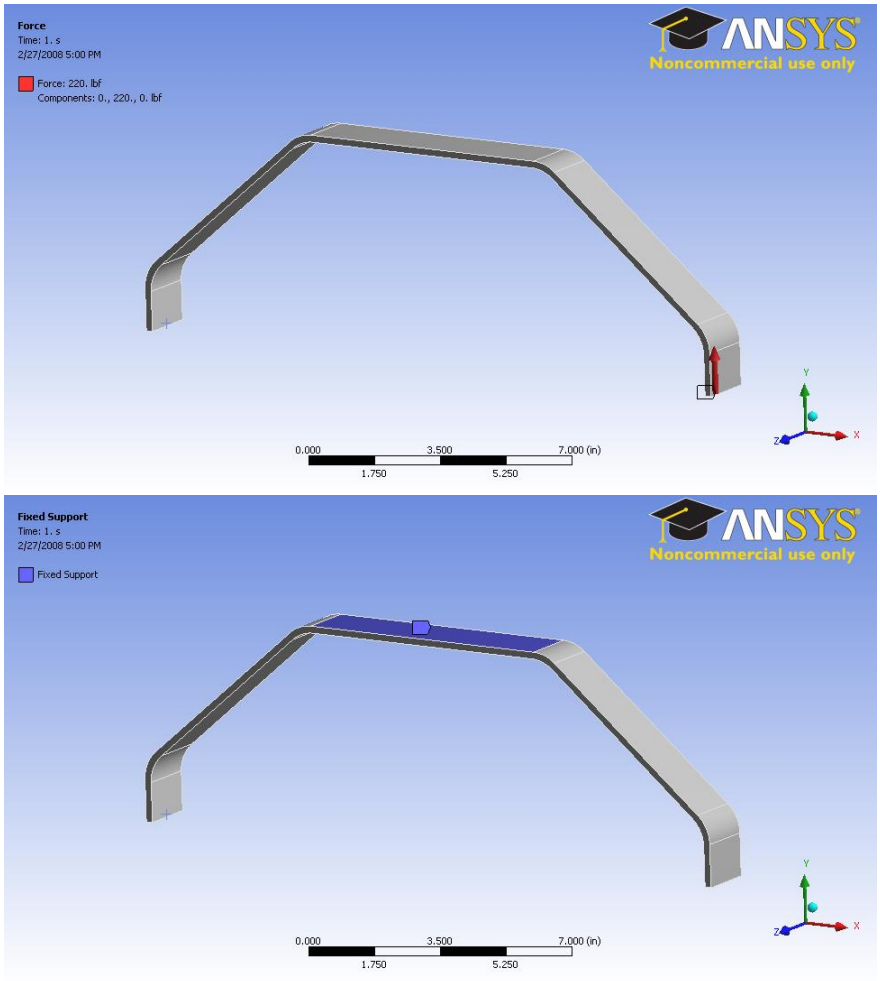

Figure 23: Loading conditions on the landing gear; ANSYS 11.0 by Dan Denmark

The loading for the landing gear consisted of placing a 290 lb force on the bottom and rigidly fixing the top.

Appendix B: Life-Long Learning

In order to achieve the goals of this design project, the team must actively engage in gaining knowledge and insight that is not part of the normal curriculum. By doing a literature search, as well as performing other research, the team can find the information they need to succeed with the project. Design concepts unique to this project, such as the tandem wing designs, and the “bow” spar design, are not specifically taught in classrooms. The team members working on these elements of the project needed to use the skills they already possessed, but also pursue additional knowledge into these subjects. Only after participating in this continued learning, were the team members able to apply their skills toward the design of these particular components to the aircraft. Though knowledge of these two aspects of the design has been obtained, there will be future instances during the course of the project where team members will have to learn additional information on the subject.

Appendix C: MATLAB Code for Take-Off Analysis

```
function [x,y]=sgy()
clear all;
clc;

%% Define values
rho=0.002378;                       %density (slugs/ft^3)
g=32.2;                             %gravity acceleration (ft/s^2)
Fc=0.03;                            %coefficient of rolling friction
T=20;                               %static thrust (lb)
z=1;                                %height difference between wings (ft)
Clmax=2.25;                         %maximum lift coefficient
Cf=0.0059;
b1=8;                               %wingspan first wing (ft)
b2=8;                               %wingspan second wing (ft)
e1=.7;                              %wing efficiency first wing (rect.)
e2=.7;                              %wing efficiency second wing (rect.)
c1=0.5;                             %Chord length first wing (ft)
c2=0.5;                             %Chord length second wing (ft)
W=55;                               %weight (pounds)
alpha=0;                            %angle of attack (degrees)
alphamax=14;
i=1;
startdist=13.083-b1-8/12;           %distance between LE of forward wing %and
                                    TE of aft wing
%% Begin While loop
while c1<=2.0
    S1=b1*c1;                       %Area (ft^2) first wing
    S2=b2*c2;                       %Area (ft^2) second wing
    AR1=b1^2/S1;                    %aspect ratio first wing
    AR2=b2^2/S2;                    %aspect ratio second wing
    y=startdist-c1-c2;              %distance between TE of forward wing
                                    %and LE of aft wing (ft)

%% Solve for Fuselage Drag
lF=49/12;                           %length (ft)
dF=6*sqrt(2)/12;                    %diameter (ft)
Swet=1300;                          %Wetted area (ft^2)
FR=lF/dF;                           %fineness ratio
FF=1+60/FR^3+.0025*FR;              %Fineness Factor
cdF=FF*Cf*Swet/(1440);              %Drag coefficient due to fuselage

%% Solve for Wing Drag
L=1.2;
R=1.05;
tc=.13;
FF=(1+L*tc+100*tc^4)*R;
cdW=FF*Cf*4;                        %Additional *2 for second wing

%% Additional Drags and solve for Cdmin (taken from Nicolai paper)
cdLG=0.0042;
cdE=0.002;
cdVT=0.00039;
```

```
cdTB=0.00009;
cdmin=cdTB+cdVT+cdE+cdLG+cdW+cdF;      %Minimum drag


%% Solve for lift and drag coefficient of first wing
cla1=1.09+0.0933*alpha;                      %coeff. of lift (infinite)
alpha_ind1=2*cla1/(pi*AR1)*(180/pi);         %induced angle of attack
cdi1=2*cla1^2/(pi*e1*AR1);                   %induced drag coefficient
alpha_eff1=alpha-alpha_ind1;                 %effective angle of attack
cl1=1.09+0.0933*alpha_eff1;                  %coeff. of lift (finite)
cd1=2*cl1^2/(pi*e1*AR1);                     %coefficient of drag

%% Solve for maximum lift on first wing
clamax1=1.09+0.0933*alphamax;
alphamax_ind1=2*clamax1/(pi*AR1)*(180/pi);
alphamax_eff1=alphamax-alphamax_ind1;
clmax1=1.09+0.0933*alphamax_eff1;

%% Solve for downwash angle on second wing
eps2=(cl1/(2*pi*AR1)*(((1+2*y/b1)/((1+2*y/b1)^2+(2*z/b1)^2))+((1-
     2*y/b1)^2)/((1-2*y/b1)^2+(2*z/b1)^2)))*180/pi;

%% Solve for lift and drag on second wing (same analysis as first)
cla2=1.09+0.0933*alpha;
alpha_ind2=2*cla2/(pi*AR2)*(180/pi);
cdi2=2*cla2^2/(pi*e2*AR2);
alpha_eff2=alpha-eps2-alpha_ind2;
cl2=1.09+0.0933*alpha_eff2;
cd2=2*cl2^2/(pi*e2*AR2);

%% Solve for maximum lift on aft wing
clamax2=1.09+0.0933*alphamax;
alphamax_ind2=2*clamax2/(pi*AR2)*(180/pi);
alphamax_eff2=alphamax-alphamax_ind2;
clmax2=1.09+0.0933*alphamax_eff2;

%% Solve for Take-off Velocity
Vto=(2*W/((S1*clmax1+S2*clmax2)*0.8*rho))^.5;

%% Solve for Mean Acceleration
D=0.5*(cd1+cdmin)*rho*(.7*Vto)^2*S1+0.5*(cd2+cdmin)*rho*(.7*Vto)^2*S2;
L=0.5*cl1*rho*(.7*Vto)^2*S2+0.5*cl2*rho*(.7*Vto)^2*S2;
a=(g/W)*(T-D-(Fc*(W-L)));

%% Solve for Take-off Distance
todist(i)=Vto^2/(2*a);           %%Take-off distance
chord(i)=c1;                     %%Chord length

%% Increment chord lengths
c1=c1+0.01;
c2=c2+0.01;
i=i+1;
end                              %end while loop
```

```
%% Plot take-off distance vs. chord length
plot(chord,todist);
grid on;
title('Take-off Distance vs. Chord Length');
xlabel('Chord Length (feet)');
ylabel('Take-off Distance (feet)');
[x,j]=min(todist);
y=chord(j);
end
```

Appendix D: Matlab code for landing force

```
g = 32.2; %ft/sec^2
w = 41; %lbs
theta = 30*pi/180; %worst case approach angle
t=0.01:0.01:1; %sec
m=w/g; %slug
v= 1.3*35 %ft/sec approximate landing velocity
f=m*sin(theta)*v./t; %lbs
vy=v*sin(theta) %vertical velocity
plot(t,f)
title('Force vs. Initial Impact Time')
xlabel('time (sec)')
ylabel('Force (lbs)')
```